Design and Analysis of a Brushless Three Phase Flux Switching Generator for Aircraft Auxiliary Power Unit

Ahmed Said Selema
Department of Electrical Engineering
Faculty of Engineering, Menoufia University
Menoufia , Egypt
ahmedselema1@yahoo.com

Mohamed Mustafa El-Shanawany
Department of Electrical Engineering
Faculty of Engineering, Menoufia University
Menoufia , Egypt
m.shanawani@yahoo.com

Dina Shaban Osheba
Department of Electrical Engineering
Faculty of Engineering, Menoufia University
Menoufia , Egypt
engdina20085@yahoo.com

Salwa Mohamed Tahoun
Department of Electrical Engineering
Faculty of Engineering, Menoufia University
Menoufia , Egypt
salwatahun@yahoo.com

***Abstract*— This paper introduces a design of a three-phase flux switching machine (FSM), which is mainly designed for a 400 HZ aircraft auxiliary power unit. In this design, there are two winding sets embedded in the stator slots. One, is referred to as three phase armature windings, supply the power to the aircraft electrical system. The other winding, namely excitation winding, is fed from a dc supply. Also, a slotted rotor will be designed without any winding or permanent magnets. Moving the field winding to the stator not only ensures brushless construction, but also reduces generator weight through the direct coupling between the generator and the gas turbine. The machine is initially simulated using 2-D finite element analysis (FEA) and its performance is analyzed. Additionally, a prototype is implemented, and its performance is practically measured in order to prove the validity of the proposed machine for aircraft auxiliary power units.**

Keywords—Brushless, flux switching generator, field excited, aircraft auxiliary power units.

I. INTRODUCTION

Nowadays, many aircrafts can generate their own power though the use of auxiliary power units (APUs). APUs are used to provide electric power to the aircraft electrical systems while the main engines are disabled. For example, running air conditioning while the aircraft is stationary on the ground. Typically, these systems consist of a small gas turbine engine connected to a wound-field synchronous generator. One of the major problems of these systems is the utilization of slip rings or brushes, which reduces the system reliability.

The brushless construction of such generation system can be fulfilled using the conventional three-stage generation system illustrated in Fig. 1. This system consists mainly of a permanent magnet generator, an exciter, and a synchronous generator. The rotors of the three stages are mounted on a common shaft and the three phase windings of the exciter are connected to a bridge rectifier fixed on the rotating shaft to supply the field winding of the synchronous generator without the use of brushes or slip rings. Although this method has high reliability, but it limits the rotor speed.

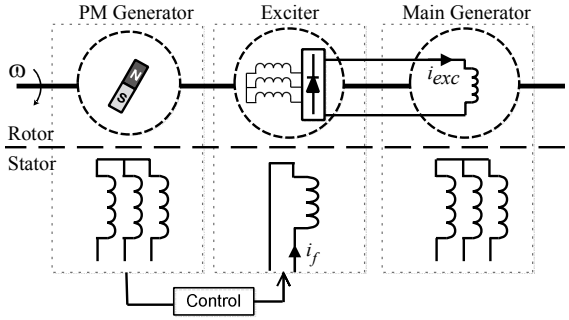

Fig. 1: The conventional three-stage brushless generation system.

Furthermore, if the excitation winding of the synchronous generator is moved to the stator, the brushless construction can be accomplished using a single-stage direct-connected machine. One of the machines which can achieve that purpose is flux switching machines (FSM).

Recently, the interest in the FSMs has been growing due to its advantages such as:

- Brushless construction, since both field and armature windings are hosted in the stator.
- Suitability for high speed operation due to passive rotor.
- Ease of cooling, since all windings are in the stator.
- Minimum weight combined with compact structure.

For such reasons, FSMs is considered a strong candidate for many industrial applications, especially those which require high power density, robustness, and high efficiency [1]. Such applications include wind power generation [2], electric vehicles [3], electric aircraft [4], Linear motors [5], and automotive applications [6].

The main Principle of the FSMs was first introduced in the 1950s as a single-phase machine [7], and as a multi-phase machine in [8]. Same as switched reluctance machines, FSMs have compact construction with a passive rotor, so they are the ability to reach high operational speed. The FSM has multiple structure configurations depending

978-1-5386-6654-8/18/$31.00©2018 IEEE

on the rotor shape which can be inward, outward, or dual rotor [9]. FSMs have three possible excitation techniques. The dc excitation can be provided by permeant magnets fitted in the stator which increases the machine's efficiency and power density. The second technique can be accomplished by using field winding which makes the machine flux more controllable. The third technique is a hybrid combination between the past two techniques which offer more improvement in the efficiency. Recently, using dc coils for excitation has become more common than using PMs due to the disadvantages of PMs such as high cost, limited resources, and the need of magnetic shielding.

In this paper, a design of a three phase FSG is presented. This design is proposed for APU to supply the aircraft electrical system during the pre-flight conditions, while the aircraft main engines are switched-off. In this machine, there are two winding groups hosted in the stator slots. One, is called excitation winding, which is connected directly to dc supply. The other winding, is referred to as three phase armature winding, supplies power to the aircraft electrical system. The machine is first simulated using 2-D finite element method. Accordingly, a prototype is implemented, and two different rotors will be designed having different pole number. The performance of both machines is practically measured and compared. The paper is arranged as follows. Section II will be devoted to the machine configuration and operation. The machine simulation and performance will be given in Section III. In Section IV, prototyping and experimentation of the proposed machine will be provided. Finally, conclusions will be provided in Section V.

II. Machine Configuration and Operation

For this design, the possible combinations of the stator-pole number N_s and the rotor-pole number N_r can be calculated as follows;

$$\begin{cases} N_s = 6mk \quad (k = 1,2,4,5,\cdots) \\ N_r = (3m \pm 2)\, k \end{cases} \tag{1}$$

Where m is the number of armature phases. Accordingly, for a 36-pole-stator three-phase FSG, the rotor can be designed with two possible pole combinations, 22 or 14 poles as illustrated in Fig. 2 [(a), (b)] respectively.

To get symmetrical back-EMF, the number of rotor and stator poles should verify the following condition [10].

$$\frac{N_r}{N_s} = \frac{odd}{even} \tag{2}$$

As can be seen, both rotor pole number combinations satisfy the pre-mentioned equation. Thus, the three-phase no-load flux linkage waveforms for both rotors will be symmetrical.

As mentioned before all windings are placed in the stator's 36 slots as shown in Fig. 2. The field excitation winding has six dc coils, each field coil is spaced by three teeth. All the six coils are connected in series to dc supply. On the other hand, the three-phase armature windings have 12 coils. Each phase has 4 coils connected in series. Each armature coil is spaced by 2 teeth. The machine winding layout is shown in Fig. 3. The machine main dimensions

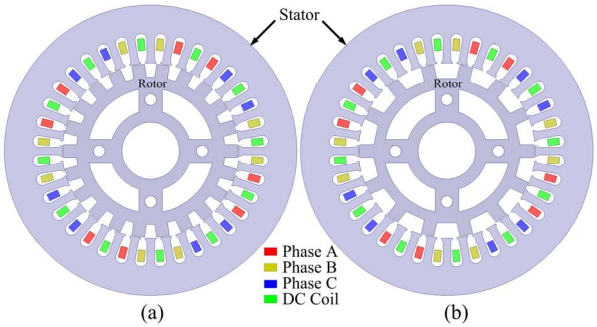

Fig. 2. Proposed FSG configuration. (a) 22-pole rotor. (b) 14-pole rotor.

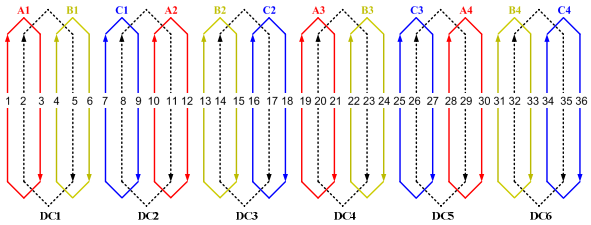

Fig. 3. The proposed FSG winding layout.

TABLE I MACHINE DIMENSION PARAMETERS

Stator		
Outer Diameter	125 mm	
Inner Diameter	75.5 mm	
Yoke Hight	12 mm	
Tooth Hight	13 mm	
Tooth Width	3.5 mm	
No. of Teeth	36	
Axial Length	73 mm	
Rotor	**Rotor (a)**	**Rotor (b)**
Outer Diameter	74.7 mm	74.7 mm
Inner Diameter	24.5 mm	24.5 mm
Slot Depth	5.8 mm	5.8 mm
Yoke Hight	5.4 mm	5.4 mm
Tooth Width	5.5 mm	5.5 mm
No. of Teeth	22	14

TABLE II MACHINE ELECTROMAGNETIC PARAMETERS

Parameter	Value
Number of armature phases	3
Rated field MMF	1320 At
Rated Field current	4 A
Turns number per armature coil	55
Turns number per field coil	55
Field wire diameter	0.6 mm
Armature wire diameter	0.6 mm
Wire current density	10.5 A/mm^2

and electromagnetic parameters are included in Table I and Table II respectively.

The no-load field distributions at the rated MMF for both rotors are illustrated in Fig 4[(a), (b)]. Moreover, the open circuit three-phase flux linkage for both 22-pole and 14-pole rotors are illustrated in Fig. 5[(a), (b)] respectively. As expected, both rotors have symmetrical waveforms with good sinusoidal patterns. The EMF frequency can be estimated as a function of the rotor pole number and the generator speed n, as described;

$$f = N_r \cdot \frac{n}{60} \tag{3}$$

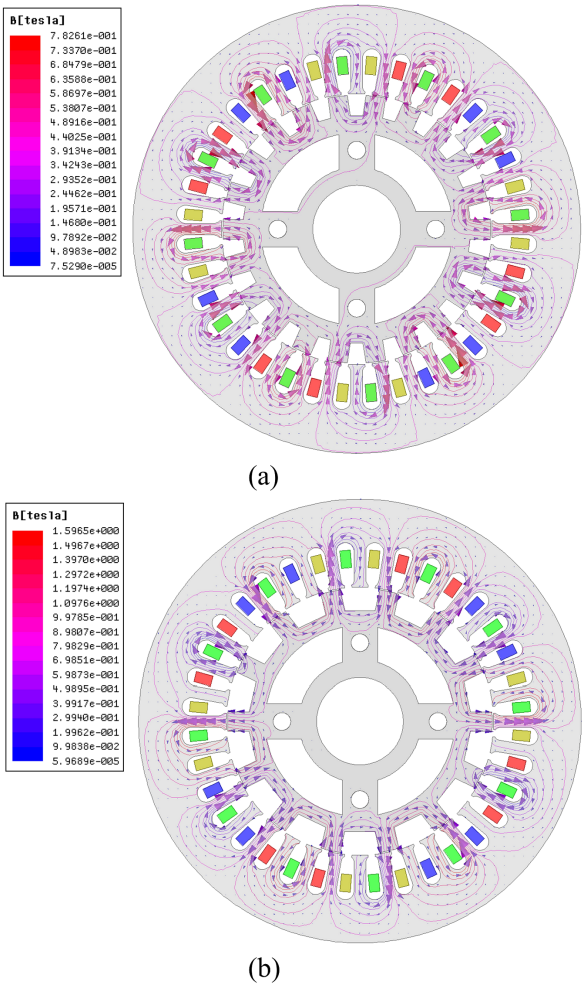

Fig. 4. Open-circuit field distributions at the rated MMF. (a) 22-pole rotor. (b) 14-pole rotor.

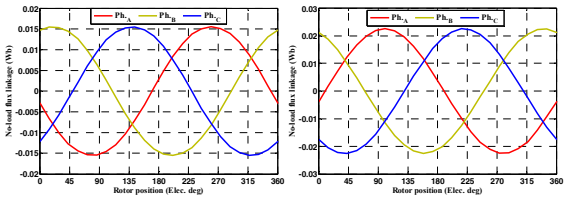

Fig. 5. Typical no-load flux linkage waveforms at the rated MMF. (a) 22-pole rotor. (b) 14-pole rotor.

Hence, in order to generate the EMF with the desired frequency of 400 Hz using the proposed FSG, the 22-pole and 14-pole rotors must rotate with a specific speed of 1090.9 RPM and 1714.3 RPM respectively. This difference in the speed will cause a corresponding difference in the generated EMF values, as will be seen in the next section.

III. Machine Simulation and Performance

In order to verify the flux switching theory, the performance of each machine is simulated using finite element method and the no-load and on-load phase output voltages are simulated at 400 Hz.

The simulated no-load three-phase back-EMF waveforms under rated conditions for both rotors are illustrated in Fig 6[(a), (b)]. As expected, the EMF waveforms are symmetrical with good sinusoidal patterns.

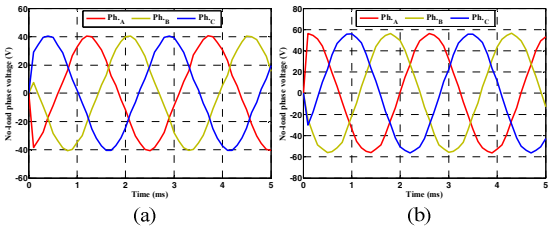

Fig. 6. The simulated open-circuit phase voltage waveforms at rated conditions. (a) 22-pole rotor. (b) 14-pole rotor.

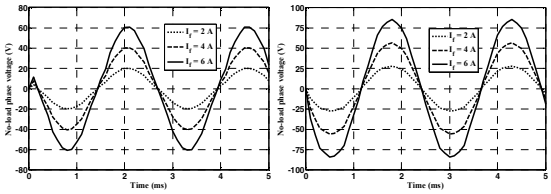

Fig. 7. The simulated no-Load phase voltage at different excitation levels. (a) 22-pole rotor. (b) 14-pole rotor.

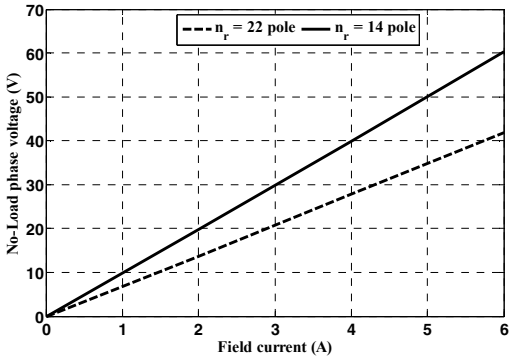

Fig. 8. The simulated no-load EMF variation with the field current at the rated speed.

Also, the no load back-EMF for both rotors is simulated at different excitation levels as shown in Fig 7[(a), (b)]. Moreover, the variation of the simulated no-load back-EMF with the field current for both rotors is illustrated in Fig. 8. As can be noticed, the EMF in case of the 14-pole rotor is about 50 % higher than that of the 22-pole rotor. That is because of the difference between the speed of each rotor at which the EMF frequency is 400 HZ.

Additionally, the on-load performance of the proposed machine at rated condition is simulated. The waveforms of the load voltage and current are shown in Fig. 9 and Fig. 10 respectively. Obviously, both voltage and current waveforms have good sinusoidal shapes. Also, the variation of the load voltage with the load current at different excitation levels is shown in Fig. 11. As can be noticed, the machine has poor voltage regulation. This problem will be solved in the next section.

IV. Prototyping and Expermentation

For the physical validation of the proposed machine in the application of aircraft auxiliary power units, a machine has been prototyped. The laminations of the stator and rotor iron parts are shown in Fig. 12. The machine stator and rotor are assembled as seen in Fig. 13(a) and (b) respectively. Also, in order to experiment the proposed FSG in the laboratory, a test bench is setup which mainly consists of a dc motor as a prime mover with its driver, the proposed FSG with a separate dc power supply for the field excitation, and

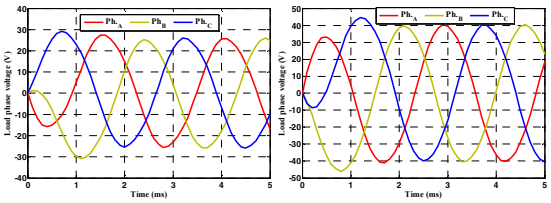

(a) (b)

Fig. 9. The simulated on-Load phase voltages at rated conditions. (a) 22-pole rotor. (b) 14-pole rotor.

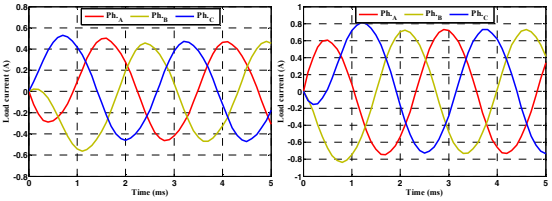

(a) (b)

Fig. 10. The simulated on-Load phase currents at rated conditions. (a) 22-pole rotor. (b) 14-pole rotor.

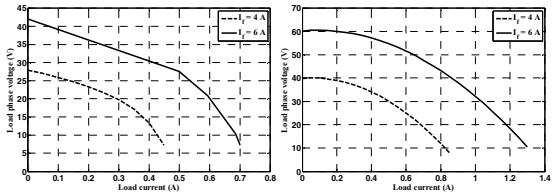

(a) (b)

Fig. 11. The simulated on-Load characteristics for different excitation levels. (a) 22-pole rotor. (b) 14-pole rotor.

a variable three phase resistance load. The experimental setup is illustrated in Fig. 14.

First, the open-circuit EMF is measured at the rated conditions for both rotors as shown in Fig. 15[(a), (b)], which have a good agreement with the simulated results shown in Fig. 6[(a), (b)]. Additionally, the no-load EMF waveforms are measured at different field currents as illustrated in Fig. 16[(a), (b)]. Also, these waveforms agree in a good way with the corresponding simulated results illustrated in Fig. 7[(a), (b)]. Moreover, the measured no-load EMF variation with the dc excitation current at the rated speed is illustrated in Fig. 17. As can be noticed, there is a mismatch between these measured results and simulated results illustrated in Fig.8. That is mainly due to the neglect of the saturation and eddy current effects in simulation.

Second, the on-load performance of the proposed machine is investigated at the rated speed for different field currents using a three-phase variable resistance load. The load voltage and load current waveforms are measured at rated conditions as shown in Fig. 18 and Fig. 19 respectively. As expected, these measure waveforms have a good agreement with the simulated waveforms illustrated in Fig. 9 and Fig. 10 respectively. Moreover, the measured on-load characteristics at different excitation levels for both rotors are shown in Fig. 20 [(a), (b)], which also agree with the corresponding simulated results illustrated in Fig. 11[(a), (b)].

Obviously, the proposed FSG suffers from some defects such as low output voltage and power. However, the desired output can be accomplished by considering a larger scale design. Moreover, one of the major problems in the prototype machine is the voltage drop on the self-inductance of the generation windings specially at this high frequency

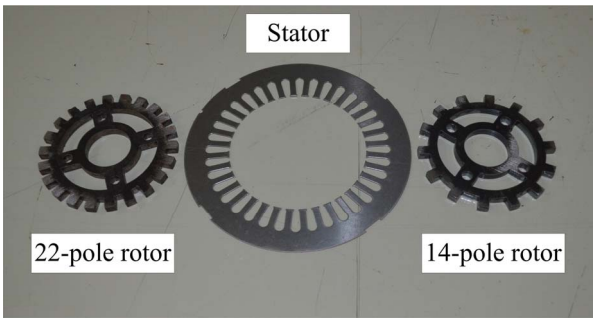

Fig. 12. The laminations of the stator and rotors.

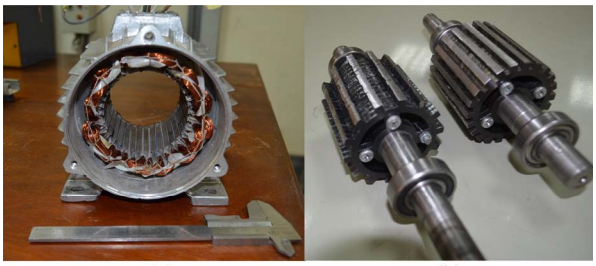

(a) (b)

Fig. 13. Prototyping of the proposed FSG. (a) assembled stator. (b) assembled rotors.

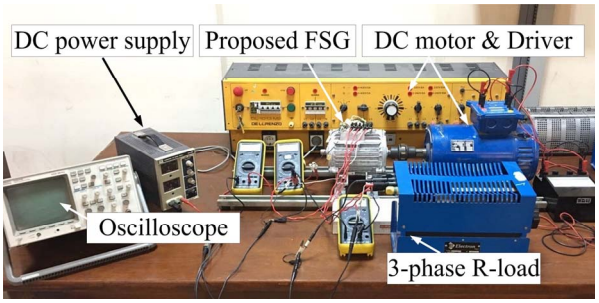

Fig. 14. Experimental setup of the proposed FSG.

operation. This problem can be solved by using a capacitor with a certain capacitance, which can be connected in series with each phase of the armature to reduce the resultant reactance, hence, increasing the output load current and power at the same output voltage. The effect of adding capacitors to the armature windings on the load characteristics is shown in Fig 21.

V. Conclusion

This paper introduces a three-phase FSG for 400 HZ aircraft auxiliary power units. Avoiding the defects of the conventional three-stage brushless synchronous generator, a direct-connected brushless generator is proposed. This can be achieved by moving the excitation windings to the stator along with the three-phase generation windings. Two different machines were studied having the same stator but with different number of rotor poles. Frist, the performance each machine is investigated using finite element analysis at no-load and on-load conditions. For physical verification, A prototype and its experimental setup is built for experimentation. Both the simulated and the measured results has a good agreement with each other. Finally, it is preferable to use the 14-pole rotor because it has higher output voltage over the 22-pole rotor case. Moreover, it was found that adding capacitors to the armature windings will enhance the output power.

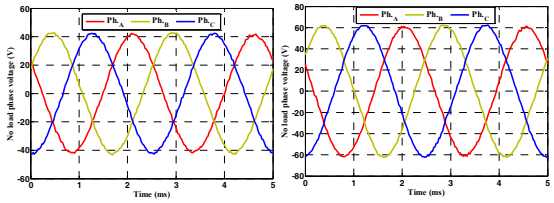

(a) (b)

Fig. 15. The measured no-Load back-EMF waveforms at rated conditions. (a) 22-pole rotor. (b) 14-pole rotor.

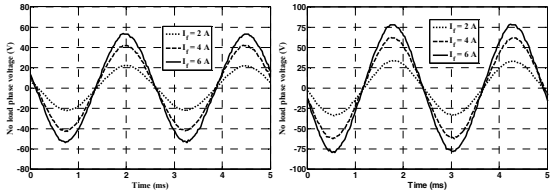

(a) (b)

Fig. 16. The measured no-Load back-EMF at different excitation levels. (a) 22-pole rotor. (b) 14-pole rotor.

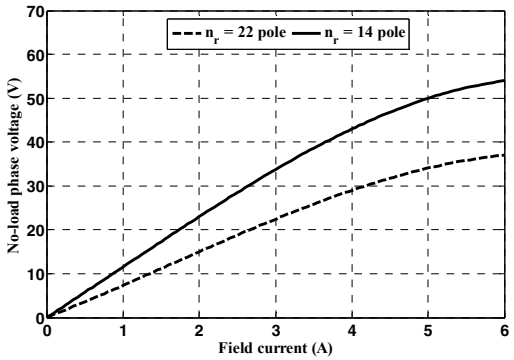

Fig. 17. The measured no-load EMF variation with the field current at the rated speed.

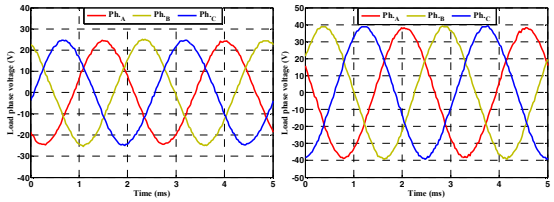

(a) (b)

Fig. 18. The measured on-Load phase voltages at rated conditions. (a) 22-pole rotor. (b) 14-pole rotor.

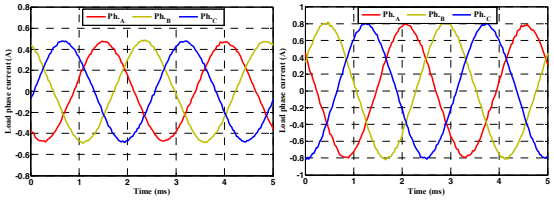

(a) (b)

Fig. 19. The measured on-Load phase currents at rated conditions. (a) 22-pole rotor. (b) 14-pole rotor.

REFERENCES

[1] B. Gaussens et al., "Magnetic field solution in doubly slotted airgap of conventional and alternate field-excited switched-flux topologies", *IEEE Trans. Magn*., vol. 49, no. 9, pp. 5083-5096, Sep. 2013.

[2] J. Cen, C. V. Nayar, and L. Xu, "Design and finite-element analysis of an outer-rotor permanent-magnet generator for directly coupled wind turbines," *Magnetic, IEEE Transactions on,* vol. 36, pp. 3802-3809, 2000.

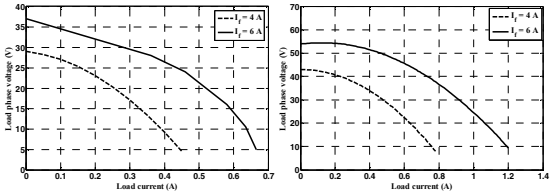

(a) (b)

Fig. 20. The measured on-Load characteristics for different excitation levels. (a) 22-pole rotor. (b) 14-pole rotor.

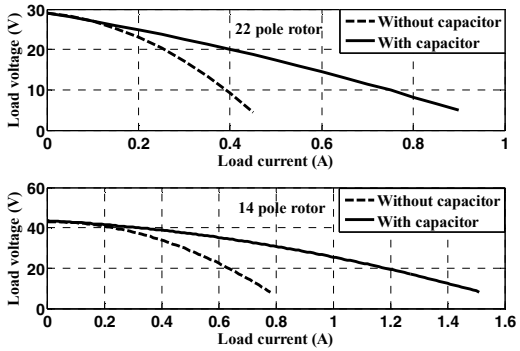

Fig. 21. The effect of adding capacitors to the armature windings on the load characteristics.

[3] E. Sulaiman, T. Kosaka, and N. Matsui, "High power density design of 6-slot 8-pole hybrid excitation flux switching machine for hybrid electric vehicles," *IEEE Trans. Magn*., vol. 47, no. 10, pp. 4453–4456, Oct. 2011.

[4] A. Nasr, S. Hlioui, M. Gabsi, M. Mairie, D. Lalevee, "Experimental investigation of a Doubly-Excited Flux-Switching Machine for aircraft DC power generation", *Proc. IEEE Int. Elect. Mach. Drives Conf*., pp. 1-7, 2017.

[5] C.-F. Wang, J.-X. Shen, Y. Wang, L.-L. Wang, and M.-J. Jin, "A new method for reduction of detent force in permanent magnet flux-switching linear motors," *IEEE Trans. Magn*., vol. 45, no. 6, pp. 2843–2846, Jun. 2009.

[6] C. Pollock, H. Pollock, R. Barron, J. Coles, D Moule, A. Court, and R. Sutton, "Flux-switching motors for automotive applications," *IEEE Trans. Ind. Appl*., vol. 42, no. 5, pp. 1177–1184, Sep./Oct. 2006.

[7] S. E. Rauch and L. J. Johnson, "Design principles of flux-switch alternators," *Trans. Amer. Inst. Electr. Eng., Power App. Syst*., Pt. III, vol. 74, no. 3, pp. 1261–1268, Jan. 1955.

[8] E. Hoang, A. H. Ben-Ahmed, and J. Lucidarme, "Switching flux permanent magnet polyphased synchronous machines," *in Proc. 7th Eur. Conf. Power Electron. Appl*., vol. 3, pp. 903–908, 1993.

[9] C. Yu and S. Niu, "Development of a Magnetless Flux Switching Machine for Rooftop Wind Power Generation," *IEEE Trans. Energy Conversion*, vol. 30, pp. 1703-1711, 2015.

[10] J. Chen, Z. Zhu, and D. Howe, "Stator and rotor pole combinations for multi-tooth flux-switching permanent-magnet brushless ac machines," Magnetics, IEEE Transactions on, vol. 44, pp. 4659-4667, 2008.